


Physical and mechanical properties of bio-modified geopolymer concrete employing bacteria

Zarina Yahya^{a,b,c}, Francesca Giuntini^d, Mohd Mustafa Al Bakri Abdullah^b,
Ana Bras^{a,*} 

^a Built Environment and Sustainable Technologies (BEST) Research Institute, Liverpool John Moores University, United Kingdom

^b Centre of Excellence Geopolymer and Green Technology (CeGeoGTech), Universiti Malaysia Perlis (UniMAP), Perlis, Malaysia

^c Faculty of Civil Engineering & Technology, Universiti Malaysia Perlis (UniMAP), Perlis, Malaysia

^d Pharmacy and Biomolecular Science, Liverpool John Moores University, United Kingdom

ARTICLE INFO

Keywords:

Biomineralisation
Ambient-cured geopolymers
Direct inclusion
Shewanella oneidensis
Self-healing

ABSTRACT

Geopolymer concrete (GPC) offers a sustainable substitute for ordinary Portland cement (OPC) concrete; yet, it has issues related to shrinkage and durability. Shrinkage in geopolymer concrete (GPC) has been reported to be 2–4 times more than that in OPC concrete, particularly when utilising calcium-rich precursors such as slag, which may further elevate the risk of corrosion in reinforced GPC. Biomineralisation, thoroughly studied in OPC concrete to enhance durability and self-healing, remains inadequately explored in GPC, particularly with the direct inclusion approach of bacteria and ambient curing conditions. This work examines the direct inclusion of bioproduct containing *Shewanella oneidensis* into GPC as a more straightforward alternative to encapsulation or carrier-based techniques. A total of 200 mL of bacterial solution was utilised to produce six cubes and six cylinders of GPC, which were cured at 15–17 °C in a laboratory environment. After 28-day period, bio-modified GPC exhibited enhanced homogeneity, a 13.1 % decrease in water absorption (from 3.06 kg/m² to 2.66 kg/m²), and a 26.5 % reduction in porosity (from 5.99 % to 4.4 %), attributed to calcite precipitation resulting from bacterial biomineralisation. Despite a minor reduction in compressive strength (from 20.44 MPa to 18.43 MPa), SEM indicated a denser matrix and improved interfacial transition zone (ITZ), while XRD validated the formation of calcite and the better preservation of quartz structures. The findings indicate that bacterial incorporation can significantly enhance the durability and self-healing capabilities of GPC, mitigating critical performance constraints. This approach demonstrates potential for sustainable infrastructure necessitating reduced maintenance and improved service life, particularly in resource-constrained or ambient-cured conditions.

1. Introduction

Geopolymer are derived from aluminosilicate precursors, such as fly ash, palm ash, metakaolin, and slag, which are sourced from industrial waste materials [1]. The geopolymer's binding characteristics are stimulated through the synthesis of precursors using an

* Corresponding author.

E-mail addresses: zarinayahya@unimap.edu.my (Z. Yahya), f.giuntini@ljmu.ac.uk (F. Giuntini), mustafa_albakri@unimap.edu.my (M.M.A.B. Abdullah), a.marmadabras@ljmu.ac.uk (A. Bras).

<https://doi.org/10.1016/j.job.2025.114799>

Received 23 July 2025; Received in revised form 17 November 2025; Accepted 27 November 2025

Available online 29 November 2025

2352-7102/© 2025 The Authors. Published by Elsevier Ltd. This is an open access article under the CC BY license (<http://creativecommons.org/licenses/by/4.0/>).

alkaline activator [2]. Many researchers have been actively conducting studies in recent years to lessen the reliance on the cement industry for building construction by utilising industry by-products. Past studies have demonstrated that geopolymer has similar physical and mechanical properties as conventional concrete, making it a potential substitute for ordinary Portland cement (OPC). Geopolymer is also more environmentally friendly in terms of carbon dioxide emissions and requires less energy usage compared to OPC production [3–6].

Geopolymer and OPC concrete exhibit fundamentally different chemical binding mechanisms, with OPC relying on hydration and geopolymer on geopolymerisation process. The hydration process in conventional concrete begins when OPC reacts with water, resulting in the formation of calcium silicate hydrate (C-S-H) and calcium hydroxide, both of which contribute to strength development [7]. On the contrary, geopolymer concrete undergoes geopolymerisation, a chemical process in which aluminosilicate precursors undergo dissolution process in an alkaline solution and then polycondensation process to create a three-dimensional sodium aluminosilicate hydrate (N-A-S-H) gel [8]. This gel acts as the binding phase that imparts mechanical strength and durability of geopolymer concrete. Nevertheless, geopolymerisation also affected by several parameters such as Si/Al and Na/Al molar ratio, activator concentration, curing temperature and calcium content [9]. Class F fly ash (low calcium), for example, is a common precursor, but its reactivity at ambient temperature is relatively slow. To achieve good early strength and a high degree of geopolymerisation, heat curing (e.g., 60–80 °C for 24–48 h) is often necessary. The amorphous glassy phases in fly ash are more resistant to dissolution of aluminosilicates and the polycondensation process at lower temperatures and the heat provides the activation energy needed for the reaction to proceed efficiently [10]. However, the requirement for heat curing can be a limitation for large-scale geopolymer concrete, cast-in-situ applications due to logistical and energy costs.

Besides that, geopolymer does have one issue, notably shrinking, particularly when employing a precursor that has a significant amount of calcium. If the shrinking problem is not addressed promptly, it may result in the formation of cracks and eventual deterioration [11]. Moreover, previous research also indicated that geopolymer concrete often shows increased chloride penetration if not well designed, particularly in chloride-rich environments [12,13]. The presence of larger or interconnected pores resulting from insufficient curing leads to a less dense geopolymer structure, hence increasing the permeability of geopolymer concrete [14]. To address this issue, adding bacteria to geopolymer can efficiently fill in the pores and improve the geopolymer's properties.

Biomineralisation has lately been recognised as a nature-inspired method for strengthening, repairing, and protection of structural materials. It involves a biological process in which microbes create minerals, primarily calcium carbonate (CaCO_3) [15]. These microbes facilitate the nucleation of CaCO_3 in close proximity to their cells where the resultant mineral deposits (CaCO_3) can effectively seal micro-cracks and micro-pores in concrete, hence enhancing its structural integrity and overall physico-mechanical properties [16]. In the field of construction materials, several techniques have been explored to incorporate bacteria into concrete to use the advantages of biomineralisation. Researchers primarily employ the encapsulation technique [15] [17,18], or the bacterial spore form due to their ability to endure extreme conditions [19,20]. Nevertheless, a drawback arises when employing spores since they necessitate germination into vegetative cells prior to actively repairing concrete cracks. Another drawback is that the utilisation of yeast extract as a germination agent adversely impacts the mechanical properties of hardened concrete [21].

The encapsulated method using hydrogel and microcapsule demonstrate satisfying results in enhancing crack healing especially for wider cracks, but these carriers are expensive [15]. Consequently, researchers have investigated the utilisation of expanded clay (EC) such as a lightweight aggregate (LWA) for the encapsulation of bacterial spores. The utilisation of EC offers more cost-effectiveness due to their natural porosity, which can enhance bacteria immobilisation and preserve bacteria spores within the concrete matrix. However, the manufacturing of EC involving a high temperature sintering process (>1000 °C), which is energy intensive [15]. Additionally, the porous nature of EC adversely affects the mechanical properties of concrete, particularly in load-bearing applications. Table 1 summarise the issues related to encapsulation techniques.

Chatterjee et al. [27] examined the efficacy of fly ash-based geopolymer mortar containing microorganisms that were subjected to harsh environments. The authors combined a bacterial solution (bioproduct) at a concentration of 10^5 CFU/mL with an alkaline activator and introduced it into the geopolymer mixture. Following a heat-curing process lasting 45 min at a temperature of 60 °C, the authors subsequently left the samples to cure under ambient conditions until the testing days. The findings demonstrate that the inclusion of bioproduct significantly enhanced the compressive, flexural, and tensile strengths of the geopolymer samples. The samples exhibited lower water absorption and enhanced resistance to chloride and sulphate attacks. The phase analysis revealed that samples containing bioproducts exhibited increased intensity in the quartz peaks. Calcite formation has been verified through the inspection of

Table 1
Summary of issues related to encapsulation techniques.

Methods of Encapsulation	Issues
Hydrogel capsule [22]	<ul style="list-style-type: none"> Bacterial spores cannot easily break through the hydrogel capsule shell unless significant cracks or degradation occur. Not cost-effective
Lightweight aggregate (LWA) [23–25]	<ul style="list-style-type: none"> Effectively healing microcracks and enhancing material resilience but LWA production involve sintering process at high temperature. The use of LWA in self-healing concrete affects the workability and mechanical properties of concrete Numerous processes (time consuming) must be undertaken before it can be utilised in mortar, despite extending the lifespan of the embedded spore in EC.
<ul style="list-style-type: none"> Embedded expanded clay (EC) with bacteria solution. Coated EC with styrene-acrylic emulsion coating to further enhance the bacteria immobilisation [26] 	

Table 2

Past studies on bio-modified geopolymer.

No	Precursors	Bacteria Type	Inclusion Mechanism	Curing	Main Outcomes	Novelty of Study
1	Metakaolin [37]	<i>Sporosarcina pasteurii</i>	Direct injection into pre-cracked samples	Ambient 24 days + sulphate + freeze-thaw cycles	CaCO ₃ as healing precipitation, improved crack closure, ettringite/calcite detected	Healing efficiency under combined sulphate + freeze-thaw exposure
2	Ground blast furnace slag + sodium silicate (SS) [35]	<i>Bacillus subtilis</i>	Mixed bacteria solution (1–3 %) with sodium silicate	Ambient curing for 7 days + observed healing process in water/air/precipitation media for 7 and 28 days	1 % bacteria solution contribute to highest compressive strength; precipitation medium most effective healing medium	Quantified effect of bacteria concentration and curing medium
3	Fly ash + NaOH (4 M) + SS [28]	<i>Sporosarcina pasteurii</i> (bacteria) + <i>Rhizopus oligosporus</i> (fungi)	Direct addition of bacteria + fungi solution (400 mL/m ³)	Moist curing at room temperature	Higher compressive strength due to combination of bacteria and fungi; calcite formation	First fungi bacteria combined system in GPC
4	Metakaolin (MK) + SS [20]	<i>Sporosarcina pasteurii</i>	Spores blended with MK	Environmental chamber curing 60 °C for 6 days and 1 day oven (60 °C) curing, pre-cracked sample at day 7, immersion in precipitation medium for 3 days	No leakage of spores; CaCO ₃ as healing product; bacteria can be added directly into geopolymer mixture without encapsulation or immobilisation.	Demonstrated spores survive inside MK geopolymer matrix
5	Fly ash + NaOH (12 M) + SS [33]	<i>B. subtilis</i> , <i>B. sphaericus</i> , <i>B. thuringiensis</i>	Direct spore suspension with activator	Oven curing 60 °C + dry-wet cycles + water immersion	Direct spore suspension with activator	First co-culture system in fly ash based geopolymer
6	Metakaolin + Slag + NaOH + SS [38]	<i>Sporosarcina pasteurii</i>	Two methods: Bacteria absorbed into MK and mixed with water	Oven curing 60 °C for 48 h, pre-cracked the samples, observed crack healing in different medium	Water absorption decreased 75 %, permeability reduced, CaCO ₃ as healing product	Absorption method of bacteria into MK
7	Fly ash + NaOH (12M) + SS [27]	<i>Bacillus subtilis</i>	Cells diluted with activator or water	Oven curing 60 °C for 45 min + ambient curing, tested for acid, chloride, sulphate, thermal resistance	Enhanced strength, acid and chloride resistance, thermal stability, bacteria viable 1 year	Demonstrated 1-year bacterial viability in GPC
8	Fly ash (Class F) + NaOH (10 M) + SS [19]	<i>Bacillus cohnii</i>	Endospores mixed with fly ash (10 ⁶ spores/g)	Air curing 90 days + water immersion + chloride/sulphate tests	CaCO ₃ sealing improved durability, reduced chloride ingress, regained 12 % strength	First to study <i>B. cohnii</i> in GPC, showing long-term chloride resistance
9	Slag + NaOH + SS [34]	<i>Bacillus pasteurii</i>	Bacteria + urea + CaCl ₂ solution mixed into GPC	Room temperature curing	CaCO ₃ improved strength up to 10 ⁵ CFU/mL; higher concentration reduced strength	Defined optimal bacteria concentration (10 ⁵ CFU/mL) for strength
10	Slag + NaOH + SS [39]	<i>Sporosarcina pasteurii</i>	Bacteria solution mixed with water during mixing process	28 days curing + exposure to elevated temperature (200–800 °C)	Samples with bacteria retained higher strength at high temperature (≤400 °C)	Explored bacterial performance at elevated temperatures
11	Metakaolin + NaOH (12M) + SS [40]	<i>Sporosarcina pasteurii</i>	Spray, injection, and immersion with bacterial culture	Room temperature curing for 28 days + 2-month healing cycles	Immersion method produced lowest water absorption, crack sealing by CaCO ₃	Compared multiple healing methods (spray, inject, immersion)
Current Study	Fly ash (class F) + NaOH (12 M) + SS	<i>Shewanella oneidensis</i>	Direct addition (200 mL bacterial solution replacing activator)	Ambient curing (15–17 °C) for 28 days	–	First study using <i>S. oneidensis</i> directly added during mixing process and cured at ambient temperature

energy dispersive spectroscopy (EDS) and X-ray diffractometer (XRD) analysis.

Wulandari et al. [28] examined the combined use of fungi (*Rhizopus oligosporus*) and bacteria (*Sporosarcina pasteurii*) at a ratio of 2:1000, utilising a total dosage of 400 mL/m³ of bacterial solution. Their work indicated that fly ash based geopolymer paste containing this bacterial solution had improved compressive strength, due to calcite precipitation resulting from microbial activity. The alteration in XRD peak, both with and without the inclusion of bacteria, mostly resulted from the formation of calcite and quartz. The reduction of mullite and zeolite in the geopolymer sample, when bacteria were added, can be attributed to the bacteria's utilisation of aluminium, hydrogen, and sodium elements for their cellular metabolism [29–32]. Furthermore, Jadhav et al. [20] found that bacteria spores can be directly incorporated into a geopolymer mixture without the need for encapsulation or immobilisation. The authors demonstrated that the bacteria spores stayed alive and remain viable in the geopolymer sample during the process of geopolymerisation.

However, Doctolero et al. [33] found that geopolymer samples containing co-cultured bacteria (*Bacillus sphaericus* and *Bacillus thuringiensis*) exhibit superior crack healing efficacy, resulting in the production of calcite as a healing substance. The co-culture of ureolytic and non-ureolytic bacteria results in a synergistic enhancement of the bacteria's mineralization activity, leading to the healing of bigger cracks. Meanwhile, in the case of the slag-based geopolymer, it was discovered that the inclusion of bacteria had beneficial effects. Specifically, positive ions like Ca²⁺ were shown to be attracted to the bacterial cell surface, which has a negative charge. Subsequently, the hydrolysis of urea resulted in the formation of ammonia and carbonate. Finally, the reaction between Ca²⁺ ions and carbonate led to the formation of calcium carbonate [34].

The process of geopolymerisation plays a crucial role in determining the characteristics of both fresh and hardened geopolymer concrete during its synthesis. The kinetics of geopolymerisation, including the presence of bacteria, were assessed by Ekinici et al. [35]. The findings suggest that while the bacteria were unaffected by the initial dissolution peak, they did cause a delay in the reaction during the second polymerisation peak [35]. The significance of the second peak lies in its direct influence on the strength growth of geopolymer. At this stage, the silicate and aluminate monomers undergo polymerisation to generate alumino-silicate oligomers, which eventually form the poly(sialate) framework [36].

Numerous studies have examined conventional methods including encapsulation techniques and the use of lightweight aggregates as carriers, which are intricate processes with numerous steps. Therefore, it is essential to develop a more straightforward method that may be readily implemented. Previous studies on bio-modified geopolymer utilising various bacterial solution inclusion methods have been summarised in Table 2 to demonstrate the relevance of the current research. The primary objective of this research was to examine the efficacy of geopolymer concrete (GPC) when the bioproduct was incorporated directly into the fresh concrete mixture without employing any encapsulation technique and without requirement for heat curing to prevent limitation for large-scale geopolymer concrete. The physical and mechanical properties of GPC samples were assessed after 28 days of ageing under ambient temperature curing conditions. The sample's morphology and characterisation were analysed through the use scanning electron microscope (SEM) with EDS, of X-ray fluorescence (XRF), and X-ray diffractometer (XRD). The finding from this study can contribute to a better understanding of the inclusion of bacteria in GPC without relying on encapsulation techniques.

2. Materials and methodology

2.1. Fly ash

This investigation utilised low calcium fly ash (class F), specifically referred to as 450N according to BS EN 450-1 [41]. The chemical composition of the fly ash, determined using XRF analysis, is provided in Table 3. The morphology and phase of the fly ash was examined using SEM and XRD as depicted in Fig. 1. The EDS analysis of fly ash showed the main elements of Si, Al, Ca and Fe which is similar pattern with XRF result. Meanwhile, in term of phase analysis the fly ash displayed amorphous to semi-crystalline phase with quartz, mullite and hematite as main phases. The particle size distribution of fly ash was illustrated in Fig. 2, where d50 (median) size of fly ash was 33.1 µm.

2.2. Alkaline activator

The synthesis of fly ash involved the use of a mixture of sodium hydroxide (NaOH) and sodium silicate (Na₂SiO₃) as the alkaline activator. The NaOH solution used had a concentration of 12 Molar and was prepared 24 h prior to the experiment by diluting NaOH pellets (supplied by Thermo Scientific) with distilled water. Sodium silicate with a specific gravity of 1.5 was supplied by Fisher Scientific.

Table 3
Chemical composition of class F fly ash.

Composition (%)	SiO ₂	Al ₂ O ₃	Fe ₂ O ₃	CaO	Na ₂ O	MgO	TiO ₂	SO ³	K ₂ O
Fly ash	51.8	26.2	8.78	3.8	1.13	1.93	0.95	0.94	3.66

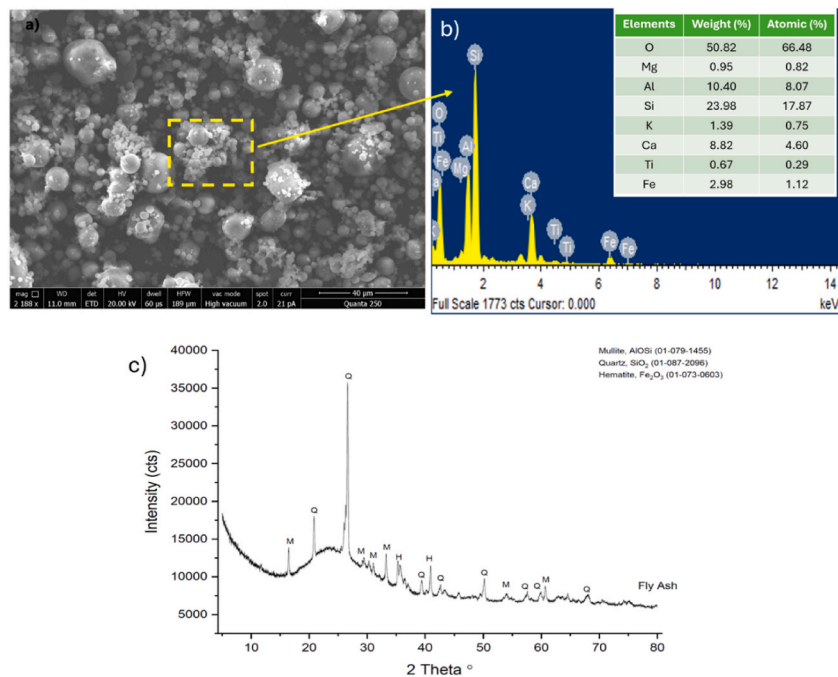


Fig. 1. (a) SEM image of fly ash, (b) EDS spectrum of fly ash, (c) XRD analysis.

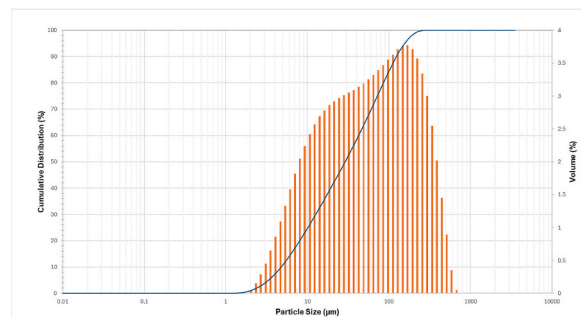


Fig. 2. Particle size distribution of fly ash.

2.3. Aggregates

The coarse aggregate used was supplied by Specialist Aggregate and Travis Perkins, UK with a size ranging from 10 to 20 mm. Sand as fine aggregates was obtained from Tarmac Plant, UK.

2.4. Preparation of bacteria solution (bioproduct)

This research utilised a strain of *Shewanella oneidensis* supplied by German company and Tryptic Soy Broth (TSB) used as a nutrient-rich medium to facilitate bacterial growth. TSB contain pancreatic digest of casein (17 g/L), papaic digest of soybean meal (3.0 g/L), sodium chloride (5.0 g/L), di-basic potassium phosphate (2.5 g/L), and glucose (2.5 g/L). The *Shewanella* strain was transferred to TSB that had been sterilised using autoclaving at 121 °C for 20 min and subsequently cooled. Following that, the bacteria culture was placed in shaking incubator for a duration of 19 h at a temperature of 30 °C and a speed of 200 rpm in order to produce a liquid bacteria solution (bioproduct). Following incubation, the number of colonies was counted using serial dilution technique, resulting in a colony-forming unit per millilitre (CFU/mL) of 10^8 CFU/mL in the bacteria solution.

2.5. Mix proportion and samples preparation

The fly ash/alkaline activator ratio and sodium silicate/NaOH ratio were maintained at a constant value of 2.0 and 2.5,

respectively. Two different groups of samples were prepared known as Control (without bioproduct) and Bio8 (with bioproduct). For each design, twelve samples were prepared (6 cubes and 6 cylinders), and the detail of materials is summarised in Table 4. A total of 200 mL of bioproduct was utilised for Bio8 samples.

The geopolymer mixture was produced by mixing fly ash, sand, and aggregate for a duration of 5 min in a concrete mixer. Subsequently, alkaline activator was added and thoroughly mixed for an additional duration of 3 min. Once the mixture achieved homogeneity, the bioproduct was added and mixed for an additional duration of 2 min as in Fig. 3. The recently bio-modified geopolymer concrete was placed into a cube mould with dimensions of 100 mm × 100 mm × 100 mm. The samples were left to cure in the laboratory with average temperature ranging from 15 to 17 °C for a duration of 28 days.

2.6. Testing procedures

2.6.1. Compressive strength

The cube samples underwent compressive strength testing after 28 days, following the guidelines of BS EN 12390-3:2009 [42]. This research presents the average values obtained from testing six samples for each design.

2.6.2. Water absorption via capillary

The capillary test was performed according to the specifications of BS EN 1015-18:2002 [43] where a total of six samples were used for this test at 28 days. The cylindrical samples were cut into a thickness of 50 mm and then subjected to an oven at a temperature of 30 °C until the alteration in mass was below 0.1 %. Subsequently, the samples were submerged in a 5 mm depth of water above the absorbent paper within a tightly sealed container to maintain a constant hydrothermal environment. The mass of the sample was recorded at 0 min, 5 min, 15 min, 30 min, 1 h, 2 h, 3 h, 21 h, 24 h, and up to 28 days or until water absorption attained a constant value.

2.6.3. Open porosity

The open porosity test was conducted based on BS EN 1936:2006 [44]. For each design, a total of six cylindrical samples measuring 50 mm in thickness and 100 mm in diameter were used for this testing. The samples were dried in the oven at 30 °C until the mass change was less than 0.1 %, and the mass was recorded as M_1 . M_2 represents the mass of samples that are saturated and submerged in water, whereas M_3 denotes the mass of samples that are saturated with water. The porosity was calculated based on Eq. (1):

$$\text{Open porosity} : \frac{M_3 - M_1}{M_3 - M_2} \times 100 \quad (1)$$

2.6.4. Electrical resistivity

The electrical resistivity was measured using a Resipod Wenner four-probe meter. For this test, cylindrical samples were used, and three measurements were taken for each sample (total of 6 samples per design), from which the average value was calculated. Electrical resistivity measurements were conducted to evaluate the potential of deterioration. Low electrical resistivity in samples elevates the probability of corrosion. Furthermore, the Resipod probe was designed in accordance with the AASHTO T 358 Surface Resistivity test method, which use surface resistivity as an indicator of concrete permeability. Four uniformly spaced probes (50 mm apart) are arranged in a straight line on the samples, with current provided to the two outside probes while the inner probes measure the resultant potential drop.

2.6.5. Microstructure assessment

2.6.5.1. Optical microscopy. The fragment of samples, post-compressive strength testing, was utilised to observe the microstructure using a Nikon microscope. The inside and outside fragments of the concrete cube, following compressive strength test, were analysed as depicted in Fig. 4.

2.6.5.2. Scanning electron microscopy (SEM) and energy dispersive spectroscopy (EDS). The morphology of the samples was examined using the FEI SEM model Inspect S50 Scanning Electron Microscope (SEM). Fragments from both the outside and inside of samples after compressive strength testing were utilised for SEM analysis. The fragments were finely sectioned and then coated with a layer of platinum. The fragments elemental composition was determined using EDS where six different spot was analysed for each fragment.

Table 4
Concrete mix design.

Concrete Composition	kg/m ³	Quantities (kg)
Fly ash	640	9.87
Coarse aggregate	864	13.32
Fine aggregate	576	8.88
NaOH solution	91.4	1.41
Na ₂ SiO ₃ solution	228.6	3.52

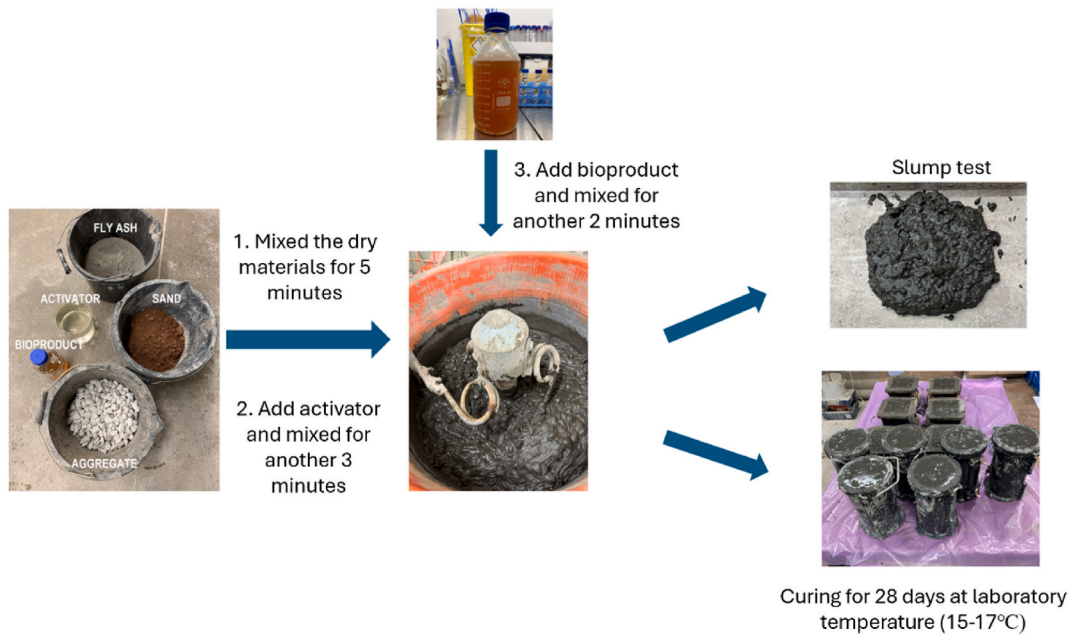


Fig. 3. Preparation of samples.

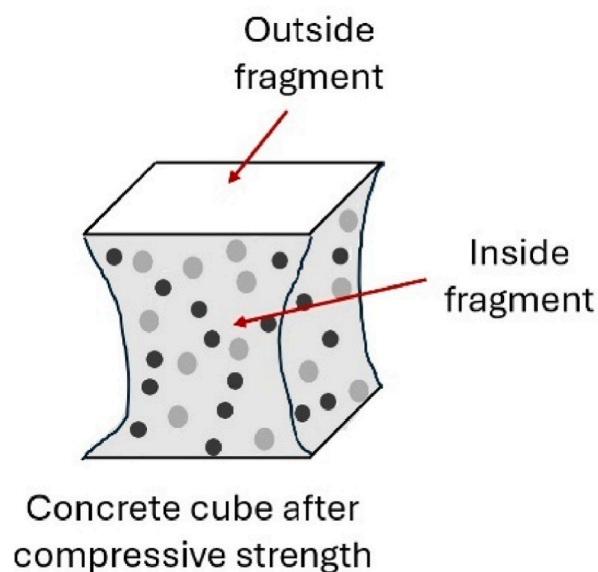


Fig. 4. Inside and outside fragment of concrete cube that used for microstructure assessment and material characterisation.

2.6.6. Material characterisation

2.6.6.1. X-ray fluorescence (XRF). The samples were pulverized into a fine powder, and the chemical composition of each mix design was analysed using the RIGAKU NEX CG II x-ray fluorescence spectrometer. The inside and outside fragment of geopolymer concrete were used to analyse the chemical composition where three samples were analysed for each design.

2.6.6.2. X-ray diffractometer (XRD). The phase analysis of raw fly ash and geopolymer samples was performed using RIGAKU MiniFlex powder X-ray diffractometer. The material was ground into a fine powder and tested within an angle range of 5° – 80° , and steps of 0.01 per second.

2.6.6.3. Differential scanning calorimeter (DSC) and thermogravimetric analysis (TGA). The Perkin Elmer DSC-6 (USA) instrument used for this analysis is located at the Science and Engineering Research Center, Universiti Sains Malaysia (USM). The samples were tested over a range a temperature range from minimum of 30 °C to a maximum of 400 °C throughout the setting duration.

TGA analyses were performed using thermogravimetric analyser (Model Perkin Elmer STA 6000, USA) to measure the mass change of a sample as well as the decomposition of calcium carbonates.

3. Result and discussion

3.1. Compressive strength, water absorption via capillary, porosity

Fig. 5(a) illustrates the compressive strength of the Control and Bio8 (geopolymer with bioproduct) at the 28-day ageing period, with the Control sample exhibiting a strength of 20.44 MPa and Bio8 demonstrating a strength of 18.43 MPa. The incorporation of bioproducts during the concrete mixing process slightly reduced the strength of geopolymer concrete by approximately 9.87 %. This reduction can be ascribed to the partial substitution of the alkaline activator with the bioproduct, potentially modifying the geopolymerisation kinetics. Moreover, a reduced availability of hydroxide ions may have slowed the dissolving of silica and alumina from fly ash, thus limiting the formation of geopolymer gel and resulting in the observed reduction in strength. Similar strength reductions have been documented in earlier research [45] when non-encapsulated or partially encapsulated bacteria disrupt matrix continuity or create weak zones in concrete. Furthermore, previous researchers [46,47], emphasised that the utilisation of low calcium fly ash as precursors necessitates heat curing at elevated temperatures (60 °C) for 24 h to attain high compressive strength at 28 days.

However, several studies have demonstrated that bacterial inclusion can increase compressive strength under various mixing circumstances. Chatterjee et al. [27] documented a maximum 15.9 % enhancement in the compressive strength of fly ash-based geopolymer with *Bacillus subtilis* attributed to calcite precipitation. Wulandari et al. [28] also observed a 43.1 % increase in compressive strength when a mixture of *Sporosarcina pasteurii* and *Rhizopus oligosporus* was introduced into fly ash-based geopolymer. Similarly, Ekinci et al. [35] reported a maximum strength increase of 118 % in slag-based geopolymer with *Bacillus subtilis*, attributed to microbial-induced calcite precipitation that acts as a filler by filling pores and cracks.

The porosity result (Fig. 5(b)) indicates a significant decrease in the Bio8 samples (4.40 %) relative to the Control (5.99 %), representing a total reduction of 26.5 %. Nonetheless, despite the reduced porosity, the Bio8 samples had slightly lower strength (18.43 MPa) in comparison to the Control (20.44 MPa). This suggests that pore refinement by bacterial biomineralisation alone was inadequate to compensate the alteration in geopolymerisation resulting from the partial substitution of the alkaline activator with bacterial solution. Based on porosity and compressive strength result, although calcite precipitation enhanced pore structure and reduced void connectivity, the disruption of gel formation and the presence of weaker interfacial transition zones constrained strength development when the samples cured at ambient temperature. Moreover, the submersion of samples in water during the open porosity test may have increased bacterial reactivity in Bio8, as water is crucial in increasing microbial metabolism and facilitating calcium carbonate (CaCO_3) formation. In the presence of water, bacteria hydrolyse urea to produce carbonate ions, which then react with calcium ions in the geopolymer pore solution to form CaCO_3 that fill pores and voids [48]. Prior research on bio-modified geopolymers also indicated that samples treated in water exhibited better physio-mechanical properties compared to those cured in air [49,50,51]. As such, the findings of current study substantiate the hypothesis that water immersion during porosity testing enhanced bacterial activity in Bio8, leading to decreased porosity despite a slight decrease in compressive strength.

A similar pattern was observed for water absorption, where after 4 days of immersion in water, a reduction (13.1 %) in water absorption was noted in Bio8 compared to the Control as illustrated in Fig. 6. The Control and Bio8 samples exhibited consistent water absorption on day 12 following water exposure. The maximum water absorption value for Bio8 samples is 2.66 kg/m^2 , while the Control sample is 3.06 kg/m^2 . Biomineralisation in Bio8 samples shown a favourable effect by filling the voids within the samples after one day of exposure to water. The availability of water for both porosity and capillary test enhanced bacterial activity, as water serves as a pathway for delivering essential nutrients for bacterial growth and metabolism.

Furthermore, the inclusion of bioproduct in the Bio8 concrete as a replacement for the activator modifies the alkali concentration

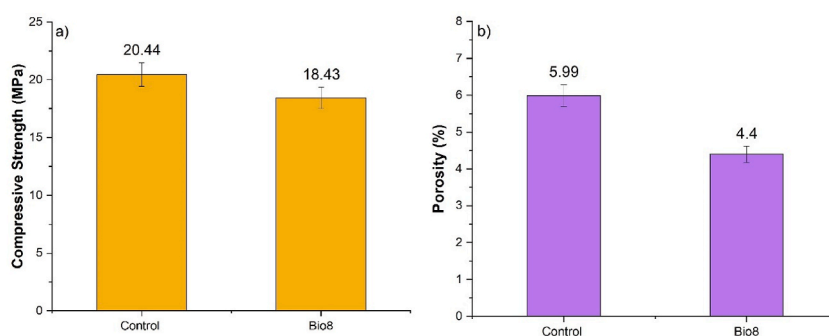


Fig. 5. (a) Compressive strength, (b) Porosity.

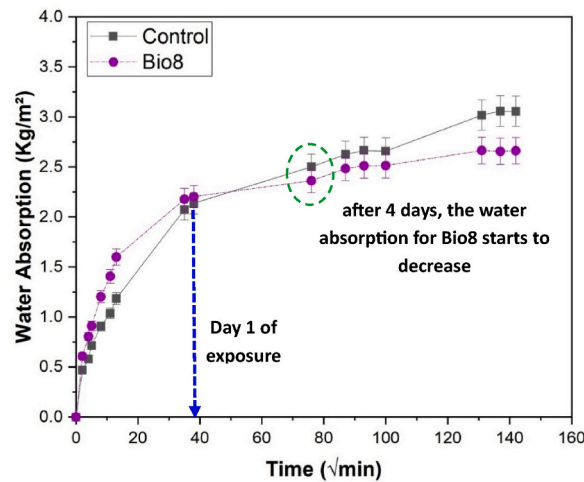


Fig. 6. Water absorption via capillary at 28 days.

and the $\text{Na}_2\text{SiO}_3/\text{NaOH}$ ratio, both of which are recognised as essential factors in controlling the geopolymerisation process. The Control sample utilised an optimally balanced activator (sodium and silicate) to enhance the dissolving of fly ash, resulting in the formation of dense geopolymer networks (N-A-S-H) that improved strength on 28 days. Despite attaining a slightly higher compressive strength, the resultant geopolymer matrix still possesses a greater number of interconnected capillary pores due to the absence of heat curing, resulting in increased water absorption. The varying water absorption between the Control and Bio8 indicates a change in pore structure and matrix densification.

The inclusion of bioproducts in Bio8 reduced the activator concentration, which impeded the geopolymerisation reaction, resulting in a marginal decrease in compressive strength. However, regarding durability characteristics such as water absorption and porosity, Bio8 demonstrates significantly lower values due to microbiological induced calcite precipitation (MICP), which fills pores with CaCO_3 . Lower alkalinity promotes bacterial metabolic activity and the production of CaCO_3 , resulting in an impermeable structure but a slightly weaker geopolymer matrix.

Consequently, the Control geopolymer employs a high alkali concentration to increase compressive strength; nevertheless, the introduction of the bioproduct (Bio8) redirects part of the chemical reaction towards healing functions, thus improving durability and self-healing capacity. The results of compressive strength, porosity, and water absorption emphasise the necessity of assessing the performance of bio-modified geopolymer not only from a strength aspect but also by considering microstructural resilience and long-term serviceability [52,53].

Based on these results, introducing bacteria to geopolymer concrete improves durability-related properties such as water absorption and porosity while slightly compromising the mechanical properties (such as compressive strength). These improvements indicate the possible application of bio-geopolymer in non-structural or durability-related components. Additional details about the impact of adding bacteria to geopolymer concrete will be included in the material characterisation subsection (SEM-EDS, XRF and

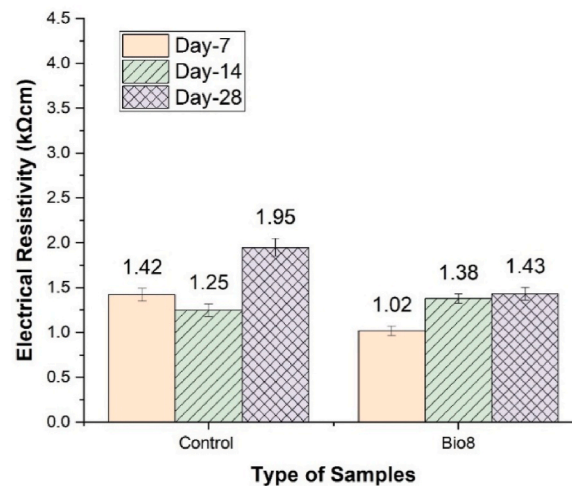


Fig. 7. Electrical resistivity at different ageing days.

XRD).

3.2. Electrical resistivity

Fig. 7 showed the surface electrical resistivity at 7, 14, and 28 days for samples both with and without bioproduct. The risk of corrosion is categorised into four categories: high risk (<10 k Ω cm), moderate (10–50 k Ω cm), low (50–100 k Ω cm), and negligible (>100 k Ω cm). Both samples exhibited low electrical resistivity, indicating a greater possibility of corrosion due to pore presence, hence enhancing fluid conductivity. Nevertheless, the value continues to increase over the ageing period, indicating that geopolymerisation continues to occur, hence improving the physical and mechanical properties of the geopolymer with time. In comparison to OPC concrete, at 28 days it recorded a reading of 15 k Ω cm which can be classified as moderate risk of corrosion [54]. Water curing is used in OPC concrete, which aids in the bacterial reactivity in filling the pores and improves the electrical resistivity measurement.

3.3. Microstructure assessment

3.3.1. Morphology

The morphology of Control and Bio8 samples were analysed using SEM at 28 days, featuring two distinct spots from both the inside and outside fragments, are shown in Figs. 8 and 9. A substantial amount of unreacted fly ash, crack lines, pores, and dense matrix was observed throughout the geopolymer matrix in both samples. The existence of pores in both samples (Control and Bio8) presumably correlates with the physically bonded water that was entrapped during the curing process. The Control sample exhibits inadequate bonding in the ITZ, characterised by extensive cracking, which may result from the sample preparation process or internal stress during compressive strength testing. Additionally, the presence of unreacted fly ash in both the inside and outside fragments emphasises inadequate geopolymerisation following 28 days of ageing at ambient temperature. The dissolution of aluminosilicate from fly ash occurs at a slower rate at ambient temperatures, resulting in less development of geopolymer gel (N-A-S-H). Consequently, the reaction remains incomplete after 28 days, and a substantial quantity of fly ash remains unreacted within the geopolymer matrix. The EDS spectra obtained from selected areas reveal that the Si/Al molar ratio for both Control and Bio8 samples surpassed 3.0, whereas previous research indicated that a Si/Al molar ratio of 3.0 is optimal for geopolymerisation. Additional clarification concerning this ratio will be provided in the subsection of molar ratio (3.4.2). Furthermore, low calcium fly ash exhibits minimal reactivity at ambient temperature owing to its predominantly amorphous glassy composition. Previous research indicated that in the absence of heat curing, the activator is less effective at dissolving this structure, hence resulting in a reduced extent of geopolymerisation [2]. Furthermore, the matrix's surroundings displayed a lack of homogeneity and a porous structure, indicating the development of a less compact gel structure and low microstructural integrity.

Similarly, the Bio8 sample displayed a comparable morphological structure, distinguished by the presence of cracks and unreacted fly ash inside a dense geopolymer matrix, as displayed in Fig. 9. The present of unreacted fly ash reduces, frequently indicating partial dissolution, which could suggest an enhancement in geopolymerisation. Bio8's geopolymer matrix showed a more uniform and dense structure, indicating a better geopolymer gel formation. Furthermore, the ITZ for both fragments is more continuous, indicating

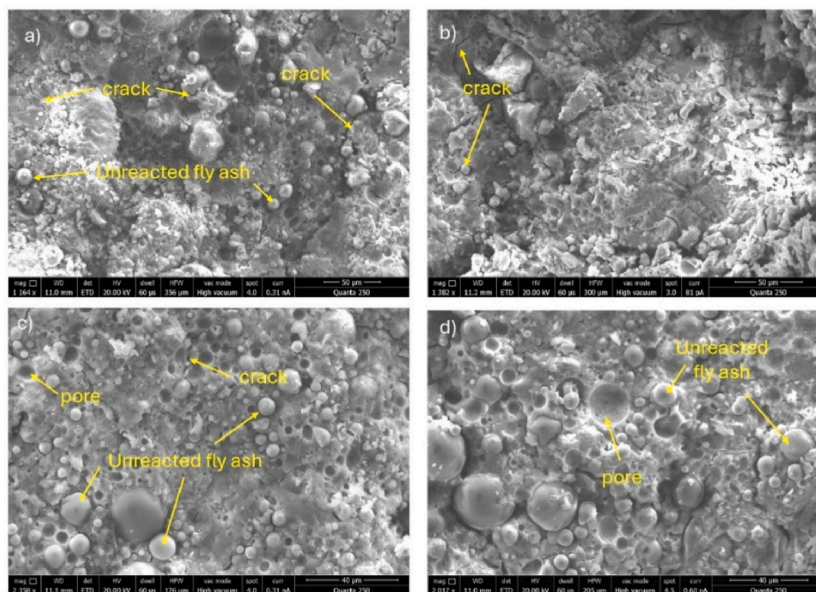


Fig. 8. SEM micrograph of Control sample (a) inside fragment, (b) inside fragment (c) outside fragment, (d) outside fragment.

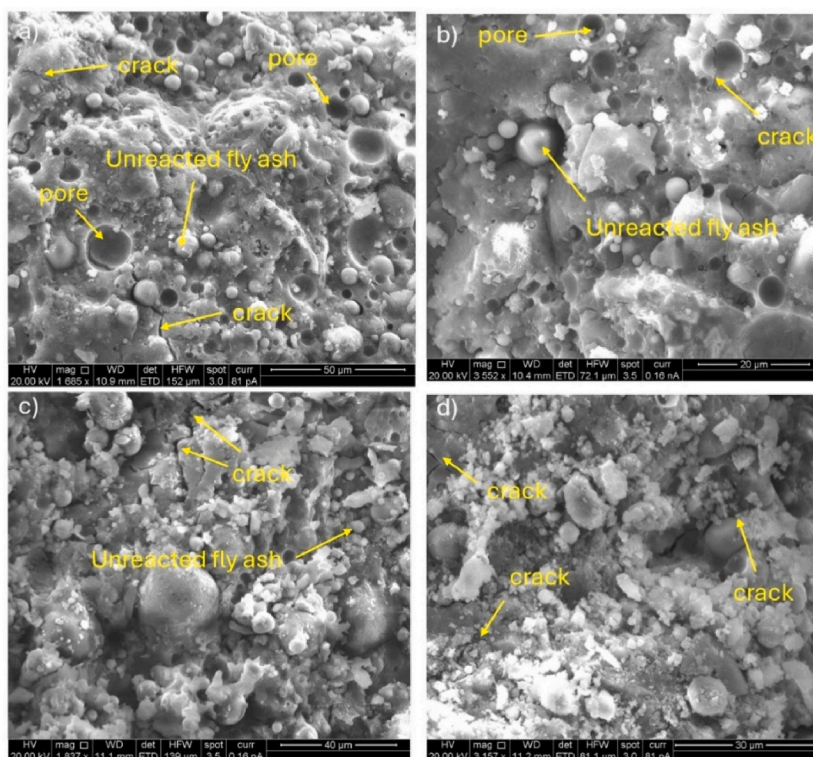


Fig. 9. SEM micrograph of Bio8 sample (a) inside fragment, (b) inside fragment (c) outside fragment, (d) outside fragment.

improved bonding between fly ash particles and the geopolymer gel. The incorporation of *Shewanella* bacteria seemingly enhances the microstructure by facilitating the densification of the geopolymer matrix and strengthening the ITZ, explaining the porosity and capillary results presented above.

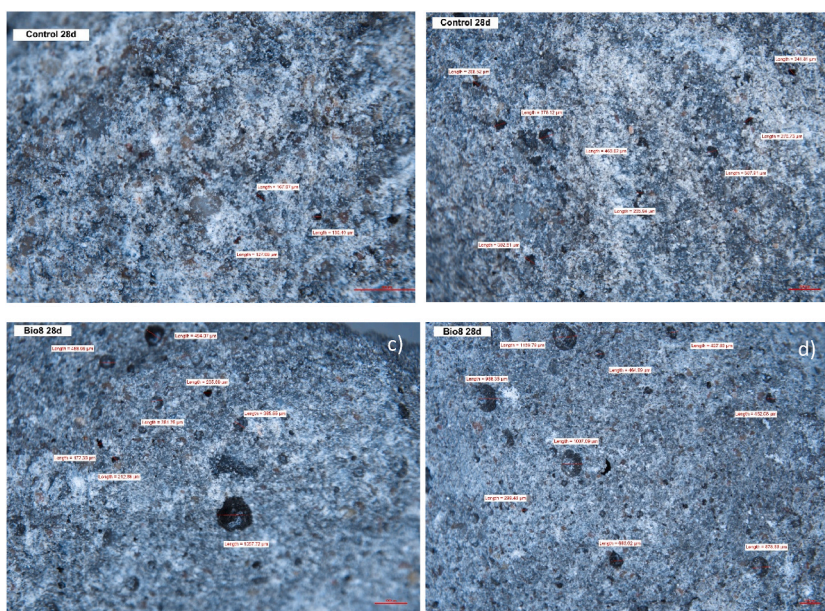


Fig. 10. The presence of pores in Control and Bio8 samples, (a) inside fragment of Control sample, (b) outside fragment of Control sample, (c) inside fragment of Bio8 sample, (d) outside fragment of Bio8 sample.

3.3.2. Microscopy images

At 28 days, the samples fragment from the compressive strength test were analysed using an optical microscope, revealing significant differences particularly in pore size distribution and ITZ. The Control sample shows small and consistently distributed pores, with sizes ranging from 127.68 μm to 167.67 μm in the inside fragment and from 241.81 μm to 465.62 μm in the outside fragment, as shown in Fig. 10. The pores seemed isolated, without evident of interconnections, indicating a rather dense and uniform matrix structure. Conversely, the Bio8 sample demonstrated an increase in pore size, particularly in the outside fragment, where the largest pore size is 1139.79 μm . The enlargement in pore size may indicate an interruption in the densification of the geopolymer matrix, maybe resulting from water loss during the ageing process or microstructural interference during geopolymerisation process. In Fig. 10 (a)–(b), some pores appeared to merge, or form elongated voids which strongly indicate the presence of interconnected pores.

Meanwhile, the ITZ of the Control sample demonstrated dense and robust bonding, indicating a substantial interaction between the geopolymer matrix and the aggregate. The Bio8 sample exhibited more pores and weak ITZ, with observable microcracks suggesting weak bonding, likely attributable to biological interference or alterations in chemical reactions caused by bacterial metabolism. These findings align with the compressive strength results, indicating that the inclusion of bacteria only improves pore refinement in the presence of water (as evidenced by porosity and water absorption results).

3.4. Material characterisation

3.4.1. Elemental analysis

Fig. 11 showed the elemental composition of the hydrated gel derived from EDS data at six selected spots (28 days), with the average values calculated for both inside and outside fragments as presented in the graph. The percentages of Si, Al, and Na in geopolymer indicate the extent of geopolymerisation. The primary elements for the development of geopolymer gel were sodium aluminate silicate hydrate (N-A-S-H) and calcium aluminate silicate hydrate (C-A-S-H), as illustrated by both samples. Despite constituting only 3.8 % of the composition, Ca nonetheless participates in the formation of the geopolymer gel. Previous research indicates that the presence of CaO in the geopolymer precursor facilitates the development of the geopolymer network and affects the setting time and properties of the hardened geopolymer concrete [55,56].

The Control samples demonstrated a higher concentration of Si and Al than Bio8, indicating a higher level of fly ash dissolution throughout the geopolymerisation process as in Fig. 11 (a). The strength of Control samples is marginally higher than Bio8 because more Si^{4+} and Al^{3+} species were dissolved in the geopolymer gel, strengthening the tetrahedral geopolymeric network. Consequently, it may be suggested that the formation of Si-O-Si linkages constituted the predominant geopolymer network in comparison to Si-O-Al and Al-O-Al bond for the Control samples. The Si-O-Si bond is recognised for its superior strength and density relative to other bonds [57]. Varying Si/Al molar ratio will lead to different geopolymer physicochemical properties. Stiff and brittle properties are found for low Si/Al ratios (<3), result in three-dimensional and cross-linked networks, making them suitable for use as cementitious and ceramic materials. Geopolymers with higher ratios (>3) result in two-dimensional and linearly linked networks with adhesive and rubbery properties (this discussion will be developed in Fig. 13 analysis).

The dissolution of fly ash during geopolymerisation in the Control sample was heterogeneous between the inside and outside of the fragment, with the outside exhibiting elevated levels of Si and Al. The outside fragment may exhibit higher concentrations of Si and Al because of exposure to or interaction with the ambient environment during the curing process.

The Ca concentration is the main difference between measurements on the materials surface (outside) or in the inner part of it, especially for Control concrete samples. Bio8 presents a homogeneous distribution of Ca in comparison to Control, indicating that the biomodification contributes to an improved composite homogeneity. The lowered calcium content in the Bio8 sample may be related to the modification in the geopolymer gel chemistry. Bacterial activity may cause the redistribution or binding of calcium in various ways, leading to a reduced measurable concentration in the internal matrix when analysed by EDS. Fig. 12 illustrated an example of Control samples in which six spots of area were utilised to measure the EDS from inside the fragment. Beside this, for Ca, the inside fragment exhibiting a larger value than the one on the outside. The synthesis of C-A-S-H appears to have occurred more internally, hence enhancing the strength of the Control samples. The Na elements from the alkaline activator exhibited elevated values for the

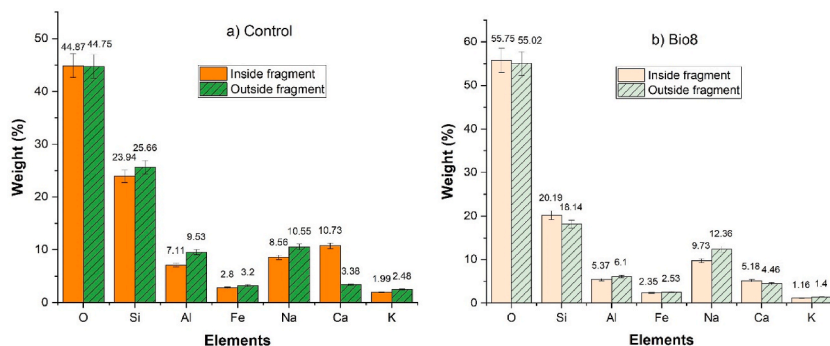


Fig. 11. EDS analysis (a) Control, (b) Bio8.

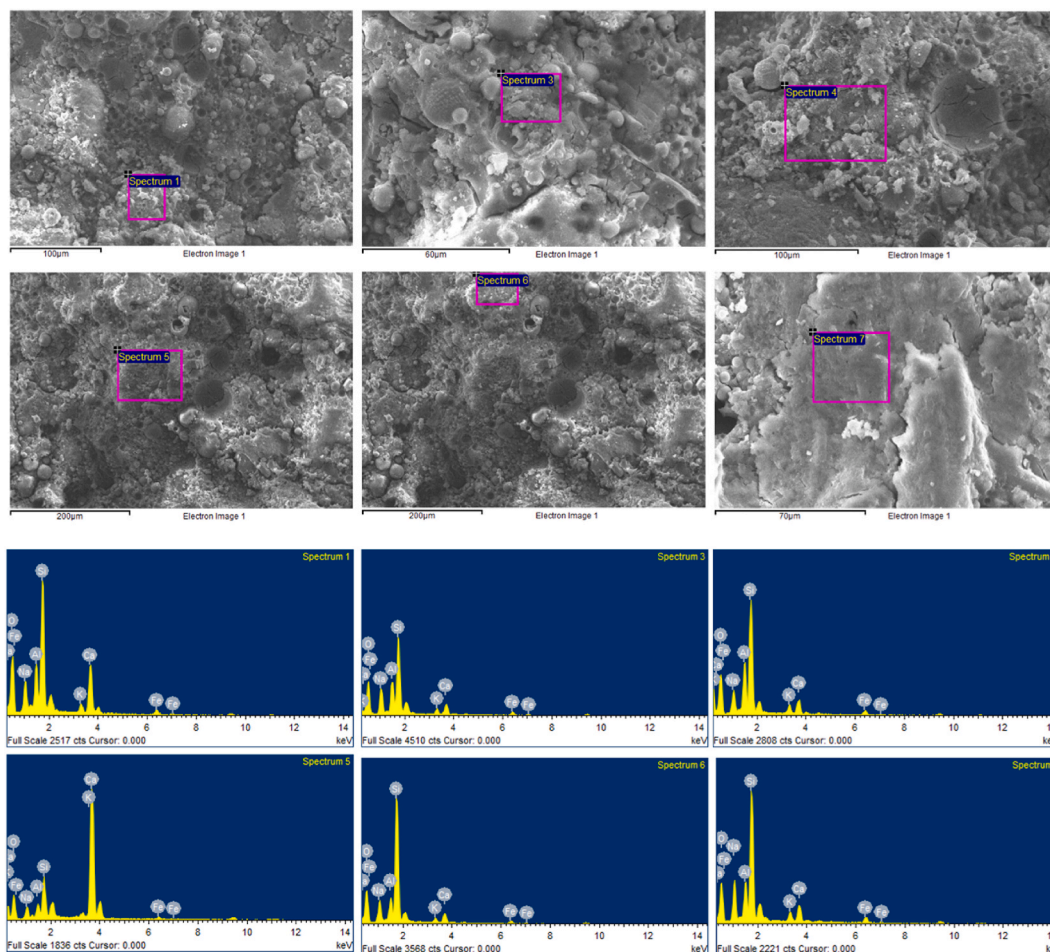


Fig. 12. Six different spots from the inside fragment of Control sample that utilised for EDS.

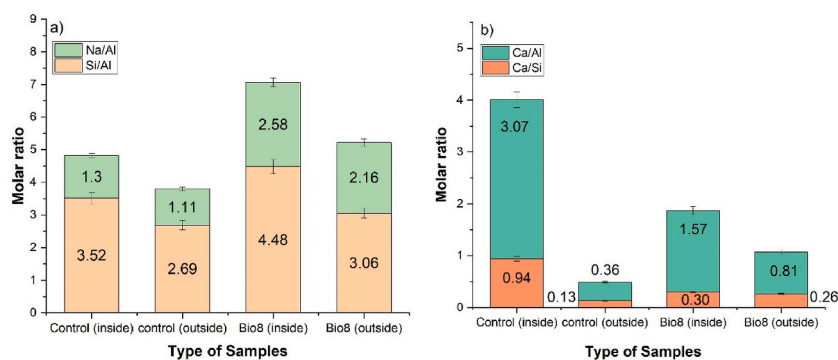


Fig. 13. (a) Si/Al, Na/Al molar ratio, (b) Ca/Al and Ca/Si molar ratio.

outside fragment, indicating that the outside fragment is more porous than the interior fragment, which facilitated the enhanced migration of Na^+ to the surface area.

The elemental compositions of Si and Al in Bio8 exhibit minor variations from Control samples, with a reduction of Si and Al noted in Bio8 compared to the Control sample. The concentration of Si was higher in the inside fragment, while Al was slightly increased in the outside fragment. The incorporation of bioproducts as substitutes for activators has altered the chemical properties of the geopolymer system by diluting the alkali concentration in the mixture. This diluting effect lowers the concentration of Na^+ and OH^- ions, as the bioproduct is more viscous and possesses a lower pH and ionic strength compared to the activator (NaOH and sodium silicate

solution). Consequently, the reduced alkalinity hindered the dissolution of aluminosilicate in fly ash and adversely affected reaction kinetics, resulting in incomplete gel formation and a reduction in the strength of the Bio8 sample compared to the Control. In addition, Bio8 had slightly greater amount of sodium (Na) than Control, especially in the outside fragment, which may indicate enhanced ionic mobility or microbial influence on alkali retention. Noushini et al. [58] state that by using appropriate curing or prolonged ageing times, Na^+ will be incorporated into the geopolymer matrix, leading to a gradual reduction in Na^+ concentration and an increase in compressive strength.

Furthermore, the oxygen concentration in the Bio8 sample shown a significant increase compared to the Control sample. This increase may be linked to elevated oxidation states and the development of secondary phases such carbonates or hydroxides resulting from microbial activity.

3.4.2. Molar ratio

The Si/Al and Na/Al molar ratios are essential to geopolymer gel, since they dictate the physical and mechanical properties of the hardened geopolymer. This section presents the molar ratios of Si/Al, Na/Al, Ca/Si, and Ca/Al derived from EDS analyses. The overall actual molar ratio from current research and past research are summarised in Table 5. Prior research has determined that the molar ratio of Si/Al between 1.0 and 3.0, and a Na/Al ratio of approximately 1.0, are ideal for the geopolymerisation process, resulting in enhanced mechanical properties of the geopolymer [2,59,60]. In Control samples, the Si/Al and Na/Al ratios ranged from 2.69 to 3.52 and from 1.11 to 1.30 as in Fig. 13(a), respectively. These ratios indicated the formation of cross-linked SiO_4 and AlO_4 tetrahedra [1, 61]. Moreover, it can be inferred that the formation of denser Si-O-Si bonds is considerably more prominent in control samples than Si-O-Al and Al-O-Al bonds. The Na/Al ratio for Control samples was marginally above one, indicating that sodium, as the cation, sufficiently balances the charge in geopolymerisation.

In the case of Bio8, the Na/Al ratio exceeded two, which disrupted the polymerisation process of the geopolymer, resulting in partial or less efficient bonding of the geopolymer gel. This can compromise the geopolymer gel structure, inhibiting the formation of a cohesive matrix when pores and cracks are present, hence weakening the mechanical characteristics. A study by Shee-ween et al. [1] discovered a comparable issue, stating that geopolymer with a greater Na/Al ratio exhibited reduced compressive strength. Additionally, the Si/Al ratio surpassed the recommended limit of 4.48 for the inside fragment, resulting in a minor reduction in strength for Bio8.

Upon comparison of the average Si/Al molar ratio of the inside and outside fragments, the Control samples exhibited the lowest value of 3.11, but the Bio8 sample recorded a value of 3.77. The enhanced rates of Al dissolution (Control samples) caused by the higher alkaline activator concentration, increased the formation of geopolymer networks and the hardened properties of geopolymer. In the case of the Bio8 sample, the addition of the bioproduct resulted in a decreased concentration of the alkaline activator, leading to a greater dissolution of Si compared to Al, hence increasing the Si/Al molar ratio. This finding concurred with Somna et al. [60].

Additionally, previous studies have asserted the involvement of calcium (Ca^{2+}) in the development of geopolymer gel, where Ca^{2+} functions as a charge-balancing agent with Na^+ . Consequently, the Ca/Al and Ca/Si molar ratios were discussed in this section. The Ca/Al molar ratio for Control samples exhibited a notable disparity when compared to Bio8, suggesting that the development of C-A-S-H was mostly localised inside the fragments of the Control samples as in Fig. 13 (b). The total amount of Ca was greater in the Control sample than in Bio8, which improved the mechanical properties of the Control samples. Simultaneously, the Ca/Si molar ratio revealed the development of calcium silicate hydrate (C-S-H), confirming the involvement of excess silicate and calcium, which are also significantly concentrated within the internal fragment.

The elemental mapping of Control and Bio8 as shown in Figs. 14 and 15 clearly showed elevated calcium (Ca) content in Bio8 (18.59 %) relative to Control (12.92 %) sample, albeit a minor decrease in carbon (C). The formation of calcium carbonate within Bio8 matrix is suggested by this compositional shift as well as the mapping image significant correlation between calcium and carbon. The elevated Ca amount align with MICP where the bacteria metabolism and localised pH encourage the formation of calcium carbonates. While HR-SEM imaging of bacterial morphology was not conducted, the combine EDS evidence and established metabolic pathways of *Shewanella* clearly suggest biomineralisation precipitation within the Bio8 geopolymer system (see Fig. 16).

3.4.3. Chemical composition analysis

The bulk chemical composition of both samples, as depicted in Fig. 14, indicated an increase in SiO_2 and Al_2O_3 in Bio8 relative to

Table 5
Summary of the molar ratio from previous and the current research.

References	Molar Ratio (from EDS analysis)			
	Si/Al	Na/Al	Ca/Si	Ca/Al
Davidovits [2]	1.0–3.0	~1.0	–	–
Guo et al. [59]	0.52–3.15	0.11–0.94	–	0.07–1.04
Liu et al. [62]	1.27–2.07	–	–	–
Ge et al. [63]	2.62–4.41	0.91–2.11	–	–
Shee-ween et al. [64]	1.66–3.57	0.58–1.38	–	–
Guo et al. [65]	–	–	0.25–2.17	–
Wang et al. [66]	1.34	–	0.21	–
Current research (Control sample)	2.69–3.52	1.11–1.3	0.13–0.94	0.36–3.07
Current research (Bio8 sample)	3.06–4.48	2.16–2.58	0.26–0.30	0.81–1.57

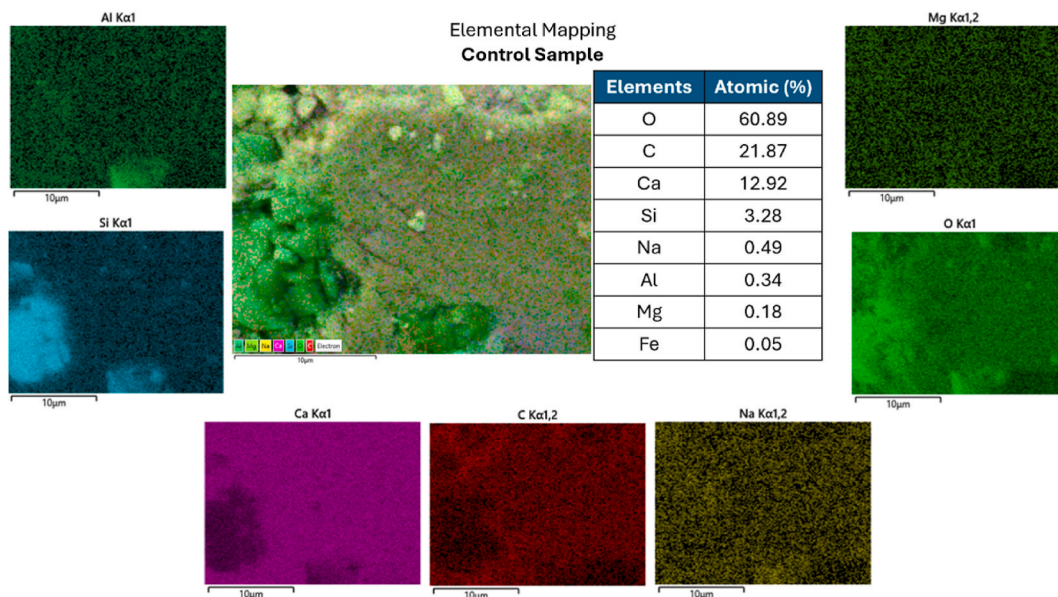


Fig. 14. Elemental mapping of Control.

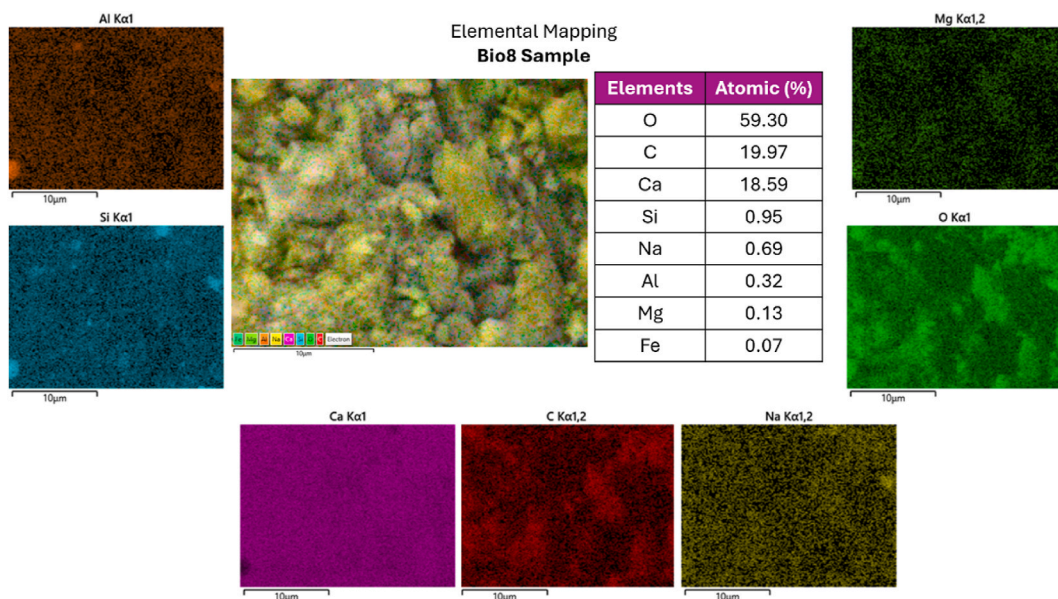


Fig. 15. Elemental mapping of Bio8.

the Control sample. This outcome differs from the EDS result, potentially attributable to disparities in the detection scale, as EDS examines surface-level and localised alterations, whereas XRF evaluates the bulk composition of the sample. The higher concentrations of SiO_2 and Al_2O_3 in the Bio8 sample suggest that the dissolution of fly ash occurs at a slower rate in Bio8, given that the initial concentrations of SiO_2 and Al_2O_3 in raw fly ash are 51.80 % and 26.20 %, respectively. The dissolution rate of fly ash was higher in the Control sample due to its higher concentration of alkaline activator. In the Bio8 sample, the incorporation of bioproduct reduced the activator concentration, resulting in a slower dissolution of the fly ash and a reduction in compressive strength.

Simultaneously, the concentration of sodium oxide (Na_2O) increases in Bio8, corroborating the EDS results. This result supports the theory of Na mobilisation induced by microbial activity, wherein the addition of bioproduct has increased the liquid content in the Bio8 sample. Furthermore, the lower concentration of activator in Bio8 results in reduced chemical incorporation of Na^+ into the geopolymer gel (N-A-S-H or C-A-S-H) [55], thus leading to a larger detection of Na_2O in the XRF analysis. Additionally, the content of iron oxide (Fe_2O_3) in Bio8 exhibited an increase compared to the Control sample, attributed to the presence of *Shewanella*, known for

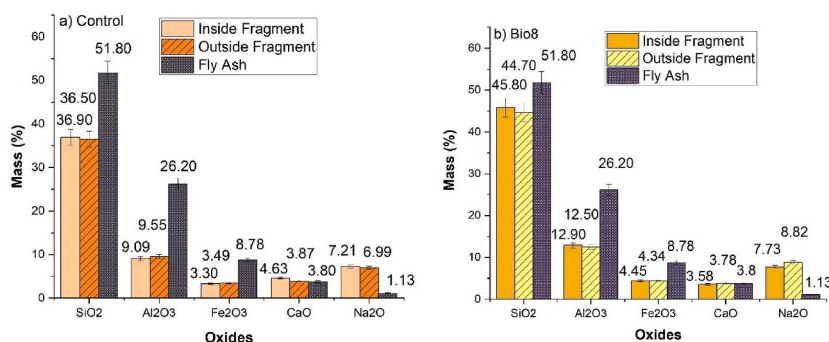


Fig. 16. XRF analysis of inside and outside fragment of (a) Control, (b) Bio8.

their interaction with iron-bearing compounds. Meanwhile, the CaO content exhibited a modest reduction in Bio8, consistent with the trend identified in the EDS data. This reduction may indicate bacterial participation in calcium consumption or its conversion into other mineral phases, which will be addressed in the phase analysis subsection.

The observed reduction in calcium content, indicated by both CaO from XRF and elemental Ca from EDS analyses in Bio8 compared to the Control, can be attributed to microbially influenced geochemical interactions within the geopolymer matrix. The inclusion of *Shewanella* likely facilitated the localised dissolution of calcium-bearing phases, supported by metabolic by-products such as organic acids or minor micro-scale acidification. These conditions can destabilise calcium-rich gels, especially C-A-S-H phases commonly exist in fly ash based geopolymers. Furthermore, microbial activity may have enhanced cation exchange processes, whereby divalent calcium ions (Ca^{2+}) are replaced by monovalent cations, particularly sodium (Na^+) [67], in agreement with the concurrent increase in sodium content indicated by both EDS and XRF data.

Furthermore, the leached Ca may have precipitated as secondary mineral phases, such as CaCO_3 , contributing to the observed reduction of Ca within the examined geopolymer matrix. Prior research by Bernal et al. [68] discovered similar occurrences, highlighting the vulnerability of reactive Ca phases to leaching under harsh conditions, whereas Achal and Pan [69] concluded that the microbially induced dissolution of Ca in concrete resulting from organic acid development. These results emphasise the complex interaction between microbial activity and the long-term chemical stability of geopolymer materials, indicating that the reduction of Ca in Bio8 is predominantly caused by microbial-driven dissolution mechanisms and cationic redistribution.

Comparing the EDS results with XRF (bulk chemical composition), the incorporation of *Shewanella* in the geopolymer concrete seems to affect elemental mobility, particularly the availability of Na, and may lead to localised microstructural dissolution of Si. Nevertheless, bulk chemical composition analysis indicates that the components remain comparatively stable, preserving their fundamental oxide framework. These findings emphasise the complex interaction between microbial activity and the chemical stability of the geopolymer matrix, especially highlighting localised alterations rather than bulk compositional changes.

3.4.4. Phase analysis

Fig. 17 illustrates the XRD overlay patterns for fly ash, Control and Bio8. The primary crystalline phases identified across all samples encompass quartz, mullite and calcite. The XRD diffractogram of class F fly ash, Control, and Bio8 samples elucidates the mineralogical alteration resulting from the incorporation of *Shewanella* bacteria into the geopolymer. The raw fly ash exhibited distinct broad humps, indicating the presence of an amorphous phase, followed by the crystalline phases of quartz (PDF no:01-087-2096) and mullite (PDF no:01-079-1455). The semi-quantitative assessment indicated that fly ash consisted of 47 % quartz and 53 % mullite, showing that the precursor material primarily comprises a crystalline aluminosilicate phase that defines low-calcium fly ash. Additionally, a broad amorphous hump was observed between 20° and 35° 2θ , confirming the presence of a significant amorphous aluminosilicate matrix, which is essential for geopolymerisation.

The Control sample retains peaks of mullite and quartz, indicating their stability post-alkali activation. The semi-quantitative data indicate that quartz increased to 67 %, while mullite dropped to 7 %, implying that a portion of the mullite and amorphous phase experienced dissolution and reprecipitation into a geopolymeric gel structure. The emergence of Albite ($\text{NaAlSi}_3\text{O}_8$) suggests the occurrence of geopolymerisation and the incorporation of cations into the aluminosilicate matrix. This newly discovered crystalline peak of albite (PDF no:01-071-1153) comprises 8 % was identified, indicating a partial transformation of the amorphous phase (raw fly ash) to the crystalline phase in the presence of a sodium-rich activator. Previous research [70] indicate that albite can improve chemical and thermal stability, hence improving the durability of geopolymer in harsh conditions.

Meanwhile, Bio8 sample exhibited significant variations in phase distribution. The intensity of the quartz peak was markedly higher than Control sample, indicating a substantially elevated semi-quantitative fraction of quartz (82 %). This indicates an elevated level of crystallinity and reduced dissolution of quartz, potentially attributable to bacterial metabolism affecting the local pH and silicate dissolution kinetics during geopolymerisation. Besides that, mullite content also increased marginally to 13 %, suggesting that bacterial presence may have partially impeded the dissolution of aluminosilicate frameworks, hence preserving a greater proportion of the original mullite structure. Nevertheless, albite peak was absent in the Bio8 sample at 28 days, suggesting that the presence of *Shewanella* may modify the sodium-aluminosilicate framework, potentially due to microbial activity or bio-mediated phase change.

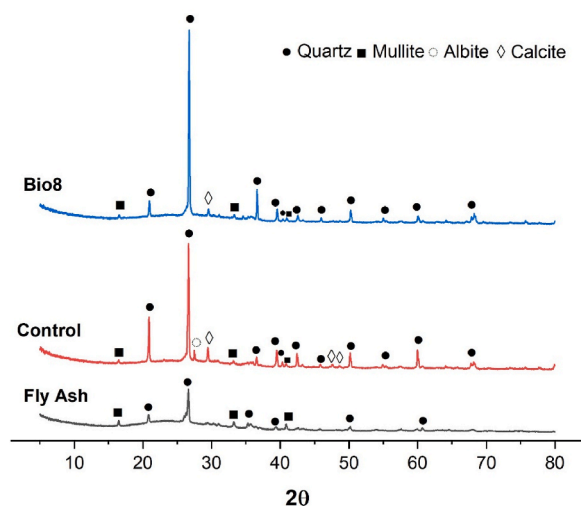


Fig. 17. XRD diffractogram.

This may elucidate why the Control sample demonstrates slightly higher compressive strength, as albite crystallisation may indicate a more complete or balanced reaction in the Control sample [71].

Regarding calcite, both samples exhibit the presence of this peak; however, the intensity of calcite (PDF no:01-072-1652) in the Bio8 (5 %) sample was marginally lower than Control (19 %). The findings may indicate that the MICP reaction produces alternative forms of CaCO_3 , such as vaterite or amorphous CaCO_3 , which possess a lower degree of crystallinity and may not be detectable in XRD analysis after 28 days of ageing. Previous research indicated that the transformation into a more crystalline calcite peak requires time [72,73].

The semi-quantitative analysis verifies that the incorporation of the bacterial solution altered the phase evolution pathway. The Control sample exhibited increased formation of secondary crystalline phases, including albite and calcite, while the Bio8 sample promoted the preservation of quartz and mullite, resulting in less crystallisation of carbonate and sodium aluminosilicate hydrate. These changes indicate the bio-mediated alteration of the geopolymerisation process, influencing the proportions of crystalline and amorphous phases, thereby modifying both microstructure and mechanical properties of geopolymer.

3.4.5. Thermal analysis

Thermogravimetric analysis (TGA) and differential scanning calorimetry (DSC) were used to analyse the phase evolution of CaCO_3 in Control and Bio8 samples. The distinct multistage mass loss pattern identified in both samples correlates with the sequential dehydration and dehydroxylation of geopolymeric gels. The TGA curve of geopolymer is divided into three zones as in Fig. 18 where zone 1 for temperatures under 200 °C, zone 2 for temperatures from 200 °C to 600 °C, and zone 3 for temperatures between 600 °C and 900 °C. In zone 1, the mass of both samples significantly decreased, signifying the evaporation of physically bound moisture inside the

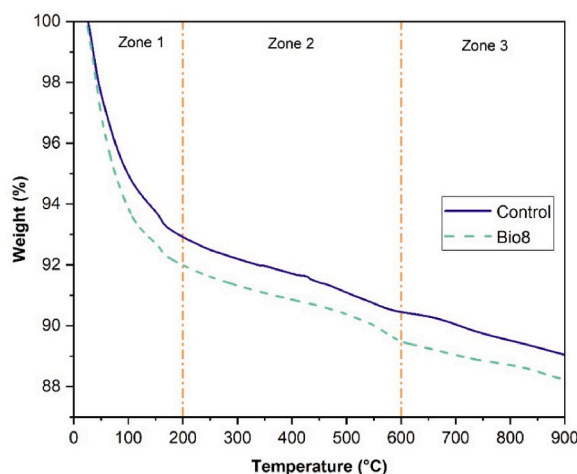


Fig. 18. TGA curves for Control and Bio8.

geopolymer framework [74]. Zone 2 pertains to the dehydration of amorphous N-A-S-H and C-A-S-H gels, as well as the dehydroxylation of more stable aluminosilicate phases. In zone 3, weight loss predominantly results from the degradation of carbonate phases [75,76], with the Bio8 sample exhibiting slightly higher mass loss (2.5 %) than the Control (1.81 %), indicating a modest increase in carbonate species.

The semi-quantitative XRD data showed that Bio8's calcite peak intensity was slightly lower than the Control's, indicating a less crystalline or more dispersed carbonate component. This finding aligns with the TGA data, which indicated very slight discrepancies in mass changes between the two samples. This suggests that bacterial activity did not substantially increase calcite precipitation but rather altered the distribution of calcium within the matrix. In Bio8, the degradation of weakly crystalline or amorphous carbonate integrated into the geopolymer gel is therefore responsible for the slightly higher mass loss.

Meanwhile, the DSC diagram as in Fig. 19 further corroborates TGA data, exhibiting extensive exothermic characteristics between 75 °C and 150 °C, which correlate to the dehydration of the amorphous gel network [74]. The Bio8 sample displayed reduce dehydration peak compared to the Control, indicative of an increased extent of amorphous phase development and enhanced structural instability. This pattern aligns with the partial substitution of the alkaline activator, wherein the bioproduct likely reduces effective alkalinity and introduces organic or ionic species that alter the reaction kinetics, so distributing the heat-release process throughout a broader range of temperatures. No discernible thermal events were seen at elevated temperatures, suggesting that bacterial inclusion affected gel formation rather than facilitating additional phase transitions.

Upon correlating with the XRD results, the minor reduction of the calcite peak observed in the Bio8 sample indicates that calcium was preferentially incorporated into the amorphous hybrid N-(C)-A-S-H framework rather than forming crystalline CaCO_3 . Moreover, the data from elemental mapping also support this finding. Bio8 sample exhibited higher calcium content compared to Control, although a lower carbon content, suggesting major proportion of calcium is bound within gel phases rather than in carbonate form. The more consistent calcium distribution in Bio8 supports the hypothesis of bacterial facilitation of ion movement and gel uniformity. The inclusion of *Shewanella* might have affected the local microenvironment during geopolymerisation by altering pH and supplying surface sites that promoted the nucleation and condensation of aluminosilicate species.

Besides that, the samples were cured at temperatures in range 15 °C–17 °C which is below the optimum metabolic range for *Shewanella*, indicating that bacterial activity was constrained to physicochemical interactions rather than active metabolism. The bacterial cells presumably functioned as passive nucleation centres, wherein functional groups on their cell walls absorbed Ca^{2+} and Na^+ ions, facilitating gel formation. As a result, *Shewanella* facilitated the formation of a more amorphous, uniformly dispersed geopolymer matrix while limiting the crystallisation of CaCO_3 .

Therefore, based on TGA, DSC, XRD and elemental mapping, it indicates that the inclusion of bacteria modified the calcium chemistry and gel structure of the geopolymer. Rather than promoting biomineralised carbonate production, *Shewanella* predominantly aided in the incorporation of calcium into the amorphous geopolymer matrix, leading to enhanced gel growth and reduced crystalline carbonate formation.

4. Conclusion

The current research examined the efficacy of *Shewanella* bacteria in enhancing GPC properties cured at ambient temperature. The result of this research improved the understanding of the impacts of incorporating bioproduct into GPC without employing encapsulating techniques.

- a) Bio8 exhibited a slight reduction in compressive strength (18.43 MPa) compared to the Control (20.44 MPa), representing a 9.87 % decrease.

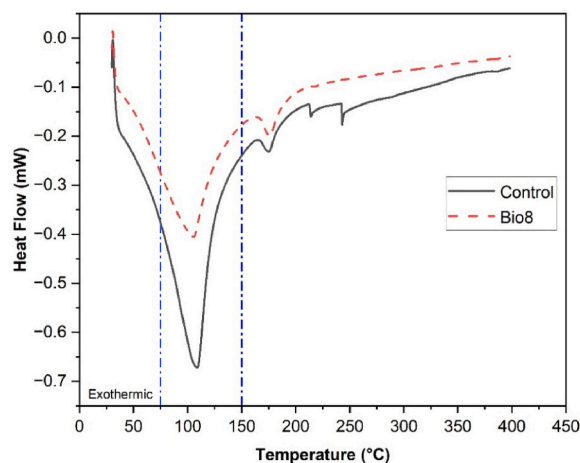


Fig. 19. DSC curves for Control and Bio8.

- b) Despite the strength loss, Bio8 showed reduced water absorption and porosity, attributed to bacterial activity and pore filling by biomineralisation products.
- c) Microstructural analysis confirmed a denser and more homogeneous matrix in Bio8, with improved ITZ continuity.
- d) Chemical and phase analyses indicated slower fly ash dissolution, higher quartz preservation, and evidence of alternative CaCO_3 influenced by bacterial activity.

This study was limited to ambient curing (15–17 °C) and a short-term evaluation at 28 days only. Meanwhile for durability indicators, were limited to water absorption and porosity. Hence, future work should investigate the effect of different curing conditions, the long-term performance of bio-modified geopolymer (60, 90, 120 and 360 days). Additionally, it is recommended also to examine the durability such as chloride penetration test and exposure to harsh environments for better understanding of the mechanism and roles of bioproduct inside geopolymer matrix.

CRedit authorship contribution statement

Zarina Yahya: Writing – review & editing, Writing – original draft, Visualization, Methodology, Investigation, Formal analysis, Data curation, Conceptualization. **Francesca Giuntini:** Writing – review & editing, Writing – original draft, Supervision, Methodology, Formal analysis. **Mohd Mustafa Al Bakri Abdullah:** Writing – review & editing, Validation. **Ana Bras:** Writing – review & editing, Writing – original draft, Visualization, Validation, Supervision, Software, Resources, Project administration, Methodology, Investigation, Funding acquisition, Formal analysis, Conceptualization.

Funding

This work is supported by the Marie Skłodowska-Curie Action (MSCA) Postdoctoral Fellowship and UK Research and Innovation (UKRI) under Engineering and Physical Sciences Research Council (EPSRC) [grant number EP/Y015959/1].

Declaration of competing interest

The authors declare that they have no known competing financial interests or personal relationships that could have appeared to influence the work reported in this paper.

Acknowledgements

The authors would like to thank Liverpool John Moores University (LJMU) and Universiti Malaysia Perlis (UniMAP) for supporting this work.

Data availability

Data will be made available on request.

References

- [1] O. Shee-Ween, et al., Green development of fly ash geopolymer via casting and pressing approaches: strength, morphology, efflorescence and ecological properties, *Constr. Build. Mater.* 398 (2023), <https://doi.org/10.1016/j.conbuildmat.2023.132446>.
- [2] J. Davidovits, *Geopolymer Chemistry and Applications*, Geopolymer Institute, 2008.
- [3] M. Nodehi, T. Ozbakkaloglu, A. Gholampour, A Systematic Review of Bacteria-based self-healing Concrete: Biomineralization, Mechanical, and Durability Properties, Elsevier Ltd, May 15, 2022, <https://doi.org/10.1016/j.jobe.2022.104038>.
- [4] X. Shi, et al., Life cycle assessment and impact correlation analysis of fly ash geopolymer concrete, *Materials* 14 (23) (2021), <https://doi.org/10.3390/ma14237375>.
- [5] W. Tang, G. Pignatta, S.M.E. Sepasgozar, Life-cycle assessment of fly ash and cenosphere-based geopolymer material, *Sustainability* 13 (20) (2021), <https://doi.org/10.3390/su132011167>.
- [6] G. Gaurav, S.C. Kandpal, D. Mishra, N. Kotoky, A comprehensive review on fly ash-based geopolymer: a pathway for sustainable future, *J Sustain Cem Based Mater* 13 (1) (2024) 100–144.
- [7] P.A.K. Nair, W.L. Vasconcelos, K. Paine, J. Calabria-Holley, A review on applications of sol-gel science in cement, *Constr. Build. Mater.* 291 (Jul. 2021) 123065, <https://doi.org/10.1016/j.conbuildmat.2021.123065>.
- [8] R. Mohamed, R. Abd Razak, M.M.A.B. Abdullah, R.K. Shuib, Subaer, J. Chaiprapa, Geopolymerization of class C fly ash: reaction kinetics, microstructure properties and compressive strength of early age, *J. Non-Cryst. Solids* 553 (2021), <https://doi.org/10.1016/j.jnoncrysol.2020.120519>.
- [9] O. Wan-En, et al., Towards greener one-part geopolymers through solid sodium activators modification, *J. Clean. Prod.* 378 (2022), <https://doi.org/10.1016/j.jclepro.2022.134370>.
- [10] A. Yılmaz, F.N. Degirmenci, Y. Aygörmec, Effect of initial curing conditions on the durability performance of low-calcium fly ash-based geopolymer mortars, *Bol. Soc. Espanola Ceram. Vidr.* 63 (4) (2024), <https://doi.org/10.1016/j.bsecv.2023.10.006>.
- [11] A. Al-Fakih, M.A.A. Mahamood, M.A. Al-Osta, S. Ahmad, "Performance and Efficiency of self-healing Geopolymer Technologies: a Review," 2023, <https://doi.org/10.1016/j.conbuildmat.2023.131571>.
- [12] J.K. Prusty, B. Pradhan, Effect of GGBS and chloride on compressive strength and corrosion performance of steel in fly ash-GGBS based geopolymer concrete, *Mater. Today Proc.* (2020), <https://doi.org/10.1016/j.matpr.2020.04.210>.
- [13] L.S. Wong, Durability Performance of Geopolymer Concrete: a Review, *MDPI*, Mar. 01, 2022, <https://doi.org/10.3390/polym14050868>.
- [14] J.L. Provis, A. Palomo, C. Shi, *Advances in Understanding alkali-activated Materials*, 2015, <https://doi.org/10.1016/j.cemconres.2015.04.013>.

- [15] P. Risdanareni, J. Wang, N. Boon, N. De Belie, Alkali activated lightweight aggregate as bacterial carrier in manufacturing self-healing mortar, *Constr. Build. Mater.* 368 (2023), <https://doi.org/10.1016/j.conbuildmat.2023.130375>.
- [16] M.V.S. Rao, V.S. Reddy, C. Sasikala, Performance of microbial concrete developed using *Bacillus subtilis* JC3, *J. Inst. Eng.: Series A* 98 (4) (2017), <https://doi.org/10.1007/s40030-017-0227-x>.
- [17] R. Alghamri, A. Kanellopoulos, A. Al-Tabbaa, Impregnation and encapsulation of lightweight aggregates for self-healing concrete, *Constr. Build. Mater.* 124 (2016), <https://doi.org/10.1016/j.conbuildmat.2016.07.143>.
- [18] X. Guo, X. Liu, S. Yuan, Effects of initial damage on self-healing of fly ash-based engineered geopolymer composites (FA-EGC), *J. Build. Eng.* 74 (2023), <https://doi.org/10.1016/j.jobbe.2023.106901>.
- [19] M. Sarkar, M. Maiti, M.A. Malik, S. Xu, Evaluation of the crack-healing performance and durability of bacteria integrated alkali-activated fly ash composites, *J. Build. Eng.* 54 (2022), <https://doi.org/10.1016/j.jobbe.2022.104642>.
- [20] U.U. Jadhav, M. Lahoti, Z. Chen, J. Qiu, B. Cao, E.H. Yang, Viability of bacterial spores and crack healing in bacteria-containing geopolymer, *Constr. Build. Mater.* 169 (2018), <https://doi.org/10.1016/j.conbuildmat.2018.03.039>.
- [21] Z. Basaran Bundur, M.J. Kirişits, R.D. Ferron, Biominedralized cement-based materials: impact of inoculating vegetative bacterial cells on hydration and strength, *Cement Concr. Res.* 67 (2015), <https://doi.org/10.1016/j.cemconres.2014.10.002>.
- [22] W. Pungrasmi, J. Intarasoontron, P. Jongvivatsakul, S. Likitlersuang, Evaluation of microencapsulation techniques for MICP bacterial spores applied in self-healing concrete, *Sci. Rep.* 9 (1) (2019), <https://doi.org/10.1038/s41598-019-49002-6>.
- [23] W. Khaliq, M.B. Ehsan, Crack healing in concrete using various bio influenced self-healing techniques, *Constr. Build. Mater.* 102 (2016), <https://doi.org/10.1016/j.conbuildmat.2015.11.006>.
- [24] H.M. Jonkers, A. Thijssen, G. Muyzer, O. Copuroglu, E. Schlangen, Application of bacteria as self-healing agent for the development of sustainable concrete, *Ecol. Eng.* 36 (2) (2010), <https://doi.org/10.1016/j.ecoleng.2008.12.036>.
- [25] M.G. Sierra-Beltran, H.M. Jonkers, E. Schlangen, Characterization of sustainable bio-based mortar for concrete repair, *Constr. Build. Mater.* 67 (PART C) (2014), <https://doi.org/10.1016/j.conbuildmat.2014.01.012>.
- [26] S. Han, I. Jang, E.K. Choi, W. Park, C. Yi, N. Chung, Bacterial self-healing performance of coated expanded clay in concrete, *J. Environ. Eng.* 146 (7) (2020), [https://doi.org/10.1061/\(asce\)ee.1943-7870.0001713](https://doi.org/10.1061/(asce)ee.1943-7870.0001713).
- [27] A. Chatterjee, A. Sarkar, S. Ghosh, S. Mandal, B. Chattopadhyay, Bacterium-incorporated fly ash geopolymer: a high-performance, thermo-stable cement alternative for future construction material, *Clean Technol. Environ. Policy* 21 (9) (2019), <https://doi.org/10.1007/s10098-019-01749-2>.
- [28] K.D. Wulandari, et al., Effect of microbes addition on the properties and surface morphology of fly ash-based geopolymer paste, *J. Build. Eng.* 33 (2021) 101596.
- [29] A.J. Cornish, R. Green, K. Gärtner, S. Mason, E.L. Hegg, Characterization of hydrogen metabolism in the multicellular green alga *Volvox carteri*, *PLoS One* 10 (4) (2015), <https://doi.org/10.1371/journal.pone.0125324>.
- [30] R.A. Cardone, et al., The Role of Sodium Hydrogen Exchanger 1 in Dysregulation of Proton Dynamics and Reprogramming of Cancer Metabolism as a Sequela, 2019, <https://doi.org/10.3390/ijms20153694>.
- [31] H.S. Titah, et al., Kinetics of aluminium removal by locally isolated *Brochothrix thermosphacta* and *Vibrio alginolyticus*, *J. Environ. Manag.* 238 (2019), <https://doi.org/10.1016/j.jenvman.2019.03.011>.
- [32] I.F. Purwanti, S.B. Kurniawan, N. 'Izzati Ismail, M.F. Imron, S.R.S. Abdullah, Aluminium removal and recovery from wastewater and soil using isolated indigenous bacteria, *J. Environ. Manag.* 249 (2019), <https://doi.org/10.1016/j.jenvman.2019.109412>.
- [33] J.Z.S. Doctolero, A.B. Beltran, M.O. Uba, A.A.S. Tigue, M.A.B. Promentilla, Self-healing biogeopolymers using biochar-immobilized spores of pure-and co-cultures of bacteria, *Minerals* 10 (12) (2020), <https://doi.org/10.3390/min10121114>.
- [34] M. Bayati, L.A. Saadabadi, Efficiency of bacteria based self-healing method in alkali-activated slag (AAS) mortars, *J. Build. Eng.* 42 (2021), <https://doi.org/10.1016/j.jobbe.2021.102492>.
- [35] E. Ekinci, İ. Türkmen, E. Birhanli, Performance of self-healing geopolymer paste produced using *Bacillus subtilis*, *Constr. Build. Mater.* 325 (2022) 126837.
- [36] P. Duxson, J.L. Provis, G.C. Lukey, S.W. Mallicoat, W.M. Kriven, J.S.J. Van Deventer, Understanding the relationship between geopolymer composition, microstructure and mechanical properties, *Colloids Surf. A Physicochem. Eng. Asp.* 269 (1–3) (2005), <https://doi.org/10.1016/j.colsurfa.2005.06.060>.
- [37] M. Ziada, H. Tanyildizi, M. Uysal, Bacterial healing of geopolymer concrete exposed to combined sulfate and freeze-thaw effects, *Constr. Build. Mater.* 369 (2023), <https://doi.org/10.1016/j.conbuildmat.2023.130517>.
- [38] B. Yilmazer Polat, M. Uysal, Bacterial crack healing in metakaolin based geopolymer mortars, *J. Build. Eng.* 39 (Jul) (2021), <https://doi.org/10.1016/j.jobbe.2021.102291>.
- [39] M. Bayati, L. Adelzade Saadabadi, A. Sedaghatdoost, Performance of self-healed alkali-activated slag mortar at elevated temperature, *J. Mater. Civ. Eng.* 35 (7) (2023), <https://doi.org/10.1061/jmce7.mteng-13977>.
- [40] H. Tanyildizi, M. Ziada, M. Uysal, N. Doğruöz Güngör, A. Coşkun, Comparison of bacteria-based self-healing methods in metakaolin geopolymer mortars, *Case Stud. Constr. Mater.* 16 (Jun) (2022), <https://doi.org/10.1016/j.cscm.2022.e00895>.
- [41] British Standards Institution BSI, BS EN 450-1:2012: fly ash for concrete - part 1: definition, specifications and conformity criteria, *British Standard* (2012).
- [42] British Standards Institution, Testing Hardened Concrete, Part 3: Compressive Strength of Test Specimens BS EN 12390-3:2009, 2009.
- [43] EN-1015-18, BS EN 1015-18: Methods of Test for Mortar for Masonry - Determination of Water Absorption Coefficient due to Capillary Action of Hardened Mortar, 3, *British Standards Institution*, 2002.
- [44] BS EN 1936:2006, Natural Stone Test Methods Determination of Real Density and Apparent Density, and of Total and Open Porosity, 2006.
- [45] A.A. Griño, H.S.P. Soriano, M.A.B. Promentilla, J.M.C. Ongpeng, Exploring the potential of polypropylene fibers and bacterial Co-Culture in repairing and strengthening geopolymer-based construction materials, *Buildings* 13 (10) (2023), <https://doi.org/10.3390/buildings13102668>.
- [46] B.V. Rangan, Fly Ash-based Geopolymer Concrete, 7, *Curtin University of Technology*, 2008.
- [47] L.B. Addis, Z.B. Sendekie, N.G. Habtu, D. de Ligny, J.A. Roether, A.R. Boccacini, Optimization of process parameters for the synthesis of class F fly ash-based geopolymer binders, *J. Clean. Prod.* 415 (2023), <https://doi.org/10.1016/j.jclepro.2023.137849>.
- [48] M.-T. Nguyen, et al., Toward self-healing concrete infrastructure: review of experiments and simulations across scales, *Chem. Rev.* (2023), <https://doi.org/10.1021/acs.chemrev.2c00709>.
- [49] E. Ekinci, İ. Türkmen, E. Birhanli, Performance of self-healing geopolymer paste produced using *Bacillus subtilis*, *Constr. Build. Mater.* 325 (Mar) (2022), <https://doi.org/10.1016/j.conbuildmat.2022.126837>.
- [50] K.D. Wulandari, et al., Effect of microbes addition on the properties and surface morphology of fly ash-based geopolymer paste, *J. Build. Eng.* 33 (Jan) (2021), <https://doi.org/10.1016/j.jobbe.2020.101596>.
- [51] E. Ekinci, İ. Türkmen, E. Birhanli, Mechanical and durability characteristics of GGBS-based self-healing geopolymer mortar produced using by an endospore-forming bacterium, *J. Build. Eng.* 57 (2022) 104944.
- [52] A. Chatterjee, A. Sarkar, S. Ghosh, S. Mandal, B. Chattopadhyay, Bacterium-incorporated fly ash geopolymer: a high-performance, thermo-stable cement alternative for future construction material, *Clean Technol. Environ. Policy* 21 (9) (2019), <https://doi.org/10.1007/s10098-019-01749-2>.
- [53] M. Sarkar, M. Maiti, M.A. Malik, S. Xu, Evaluation of the crack-healing performance and durability of bacteria integrated alkali-activated fly ash composites, *J. Build. Eng.* 54 (2022), <https://doi.org/10.1016/j.jobbe.2022.104642>.
- [54] U.U. Jadhav, M. Lahoti, Z. Chen, J. Qiu, B. Cao, E.H. Yang, Viability of bacterial spores and crack healing in bacteria-containing geopolymer, *Constr. Build. Mater.* 169 (2018), <https://doi.org/10.1016/j.conbuildmat.2018.03.039>.
- [55] G. Saini, U. Vattipalli, Assessing properties of alkali activated GGBS based self-compacting geopolymer concrete using nano-silica, *Case Stud. Constr. Mater.* 12 (2020), <https://doi.org/10.1016/j.cscm.2020.e00352>.
- [56] S. W. Wijaya Antoni, D. Hardjito, Factors affecting the setting time of fly ash-based geopolymer, *Mater. Sci. Forum* (2016), <https://doi.org/10.4028/www.scientific.net/MSF.841.90>.

- [57] E. Mohseni, Assessment of Na₂SiO₃ to NaOH ratio impact on the performance of polypropylene fiber-reinforced geopolymer composites, *Constr. Build. Mater.* 186 (2018), <https://doi.org/10.1016/j.conbuildmat.2018.08.032>.
- [58] A. Noushini, A. Castel, J. Aldred, A. Rawal, Chloride diffusion resistance and chloride binding capacity of fly ash-based geopolymer concrete, *Cem. Concr. Compos.* 105 (2020), <https://doi.org/10.1016/j.cemconcomp.2019.04.006>.
- [59] X. Guo, H. Shi, W.A. Dick, Compressive strength and microstructural characteristics of class C fly ash geopolymer, *Cem. Concr. Compos.* 32 (2) (2010), <https://doi.org/10.1016/j.cemconcomp.2009.11.003>.
- [60] K. Somna, C. Jaturapitakkul, P. Kajitvichyanukul, P. Chindaprasirt, NaOH-activated ground fly ash geopolymer cured at ambient temperature, *Fuel* 90 (6) (Jun. 2011) 2118–2124, <https://doi.org/10.1016/J.FUEL.2011.01.018>.
- [61] P. Shekhawat, G. Sharma, R.M. Singh, Microstructural and morphological development of eggshell powder and flyash-based geopolymers, *Constr. Build. Mater.* 260 (Nov. 2020) 119886, <https://doi.org/10.1016/J.CONBUILDMAT.2020.119886>.
- [62] J. Liu, et al., Correlation between dissolubilities of Si, Al, and Fe from aluminosilicate precursor and strength of fly ash-based geopolymer, *Constr. Build. Mater.* 393 (2023), <https://doi.org/10.1016/j.conbuildmat.2023.132107>.
- [63] X. Ge, X. Hu, C. Shi, The effect of different types of class F fly ashes on the mechanical properties of geopolymers cured at ambient environment, *Cem. Concr. Compos.* 130 (2022), <https://doi.org/10.1016/j.cemconcomp.2022.104528>.
- [64] O. Shee-Ween, et al., Green development of fly ash geopolymer via casting and pressing approaches: strength, morphology, efflorescence and ecological properties, *Constr. Build. Mater.* 398 (2023), <https://doi.org/10.1016/j.conbuildmat.2023.132446>.
- [65] S. Guo, C. Ma, G. Long, Y. Xie, Cleaner one-part geopolymer prepared by introducing fly ash sinking spherical beads: properties and geopolymerization mechanism, *J. Clean. Prod.* 219 (2019), <https://doi.org/10.1016/j.jclepro.2019.02.116>.
- [66] Y. Wang, R. Xiao, W. Hu, X. Jiang, X. Zhang, B. Huang, Effect of granulated phosphorus slag on physical, mechanical and microstructural characteristics of class F fly ash based geopolymer, *Constr. Build. Mater.* 291 (2021), <https://doi.org/10.1016/j.conbuildmat.2021.123287>.
- [67] J. Luo, et al., Interactions of fungi with concrete: significant importance for bio-based self-healing concrete, *Constr. Build. Mater.* 164 (2018), <https://doi.org/10.1016/j.conbuildmat.2017.12.233>.
- [68] S.A. Bernal, et al., Binder chemistry – high-calcium alkali-activated materials, in: J.L. Provis, J.S.J. van Deventer (Eds.), *Alkali Activated Materials: State-Of-The-Art Report*, RILEM TC 224-AAM, Springer Netherlands, Dordrecht, 2014, pp. 59–91, https://doi.org/10.1007/978-94-007-7672-2_3.
- [69] V. Achal, X. Pan, Characterization of urease and carbonic anhydrase producing bacteria and their role in calcite precipitation, *Curr. Microbiol.* 62 (3) (2011), <https://doi.org/10.1007/s00284-010-9801-4>.
- [70] N. Kozhukhova, M. Kozhukhova, I. Zhernovskaya, V. Promakhov, The correlation of temperature-mineral phase transformation as a controlling factor of thermal and mechanical performance of fly ash-based alkali-activated binders, *Materials* 13 (22) (2020), <https://doi.org/10.3390/ma13225181>.
- [71] H. Xu, J.S.J. Van Deventer, Geopolymerisation of multiple minerals, *Miner. Eng.* 15 (12) (2002), [https://doi.org/10.1016/S0892-6875\(02\)00255-8](https://doi.org/10.1016/S0892-6875(02)00255-8).
- [72] O. Šovljanski, et al., Comprehensive profiling of microbiologically induced caco3 precipitation by ureolytic bacillus isolates from alkaline soils, *Microorganisms* 9 (8) (2021), <https://doi.org/10.3390/microorganisms9081691>.
- [73] L.A. Ivanova, et al., Structure evolution of CaCO₃ precipitates formed during the bacillus cereus induced biomineralization, *Minerals* 13 (6) (2023), <https://doi.org/10.3390/min13060740>.
- [74] N. Hui-Teng, et al., Comparison of thermal performance between fly ash geopolymer and fly ash-ladle furnace slag geopolymer, *J. Non-Cryst. Solids* 585 (2022), <https://doi.org/10.1016/j.jnoncrysol.2022.121527>.
- [75] E. Ul Haq, S.K. Padmanabhan, A. Licciulli, In-situ carbonation of alkali activated fly ash geopolymer, *Constr. Build. Mater.* 66 (2014), <https://doi.org/10.1016/j.conbuildmat.2014.06.012>.
- [76] P. Chindaprasirt, U. Rattanasak, Calcium wastes as an additive for a low calcium fly ash geopolymer, *Sci. Rep.* 13 (1) (2023), <https://doi.org/10.1038/s41598-023-43586-w>.